Proceedings of the
47th IEEE Conference on Decision and Control
Cancun, Mexico, Dec. 9-11, 2008

TuA18.3

Robust Adaptive Control of a Twin-Rotor Aircraft

P. Krishnamurthy, F. Khorrami, Q. Lam

Abstract— We propose robust adaptive control designs for a twin-rotor aircraft with specific focus on attaining good disturbance attenuation properties to facilitate operation in a shipboard environment wherein the aircraft is subject to severe aerodynamic disturbances including ship airwake, deck vortices, and rotor downwash especially during ship roll and pitch motions. Furthermore, the controllers can operate on their own or can gracefully co-exist with a baseline controller in a control augmentation fashion thus minimizing flight software change impact. The performance of the proposed controllers was validated through extensive simulation studies.

I. INTRODUCTION

The control of rotorcraft operating under severe aerodynamic disturbance conditions is a challenging problem [1–5]. It has been noted that conventional designs of the Flight Control System (FCS) which address operations over land do not suffice in the case of shipboard operations at sea. In this paper, we propose two control approaches for a twin-rotor aircraft (for instance, the Bell XV-15 and the Bell/Boeing V-22 Osprey) with particular focus on flight operations in close proximity to ships. The proposed controllers are designed to operate as augmentation controllers (as shown in Figure 1) in conjunction with the existing FCS (nominally a PID controller of the structure shown in Figure 2). The requirement of an augmentation controller is most critical in the attitude control block whereas the performance of the baseline roll/pitch command generator and the baseline altitude controller are, in general, adequate. The controllers are based on nonlinear robust and adaptive control techniques; the first approach (Section III) is based on nonlinear adaptive control using backstepping and Input-to-State Stability (ISS) concepts while the second approach (Section IV) is based on the θ-D technique to obtain approximate solutions to a State Dependent Riccati Equation (SDRE) in real-time with low computational complexity.

The controllers have been tested and validated through extensive simulation studies; the simulation platform includes all major components of the real rotorcraft operating environment (i.e., a six degree-of-freedom model of the twin-rotor aircraft including rotor models, a six degree-of-freedom model of the ship, aerodynamic interactions between the ship and the rotorcraft, and a pilot-in-the-loop model) thus providing a reasonable fidelity of the simulation. The overall dynamic system formed by a rotorcraft operating in a shipboard environment has multiple components as illustrated in Figure 3. The core of the dynamic system which forms the focus of control design in this effort is the six degree-of-freedom (DOF) dynamic model of the twin-rotor aircraft. It is demonstrated through simulation studies in Section V that the proposed FCS designs offer significant disturbance attenuation improvements over the existing baseline controller and provide robustness to severe aerodynamic interactions such as ship airwake, deck vortices,

The first author is with IntelliTech Microsystems, Inc. (IMI), Bowie, MD, 20715. The second author is with IMI and with Control/Robotics Research Laboratory (CRRL), Department of Electrical and Computer Engineering, Polytechnic University, Brooklyn, NY, 11201. The third author is a Chief Scientist with Orbital Sciences Corporation, Dulles, VA, 20166. Emails: pkrishnamurthy@imicro.biz, khorrami@smart.poly.edu, Lam.Quang@orbital.com

and rotor downwash especially during ship roll and pitch motions, thus significantly enlarging the operational envelope of ship and rotorcraft motions and wind conditions. The utilization of the proposed augmentation controllers offers better tracking performance and disturbance rejection, adaptation to changes in environmental conditions and operating characteristics, greatly reduced computational complexity compared to SDRE based controllers, and reduced pilot workload.
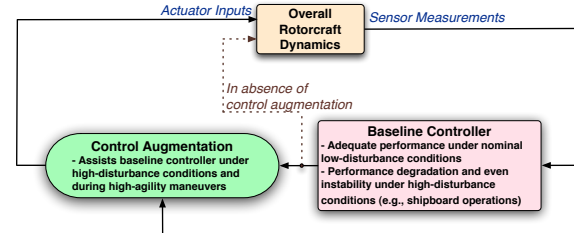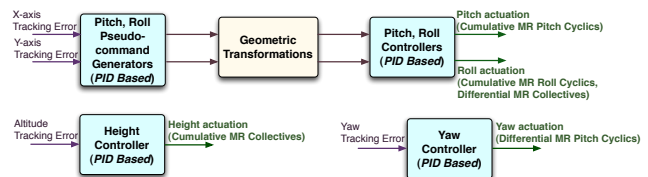

Fig. 1. Control augmentation.

Fig. 2. Structure of the baseline controller for the twin-rotor aircraft.
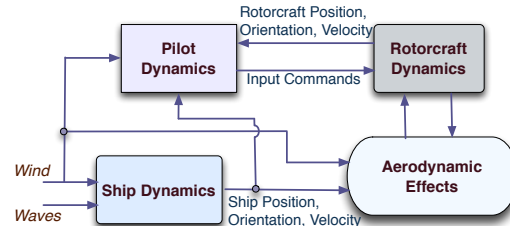

Fig. 3. Structure of the overall system model.

II. MODELING

In this section, the six degree-of-freedom dynamic model of a twin-rotor aircraft (with a left rotor and a right rotor - designated as MR1 and MR2, respectively) is described briefly. The structure of the dynamic model is illustrated in Figure 4. Following the Heffley modeling approach [6], the six degree-of-freedom dynamic model of the aircraft is developed with 17 states, namely the translational position (x, y, z) measured in earth-frame (in feet), the translational velocity (v_{bx}, v_{by}, v_{bz}) measured in body-frame (in feet/sec), the angular position, i.e., roll (θ_x), pitch (θ_y), yaw (θ_z) (in radians), the angular velocity $(v_{b\theta_x}, v_{b\theta_y}, v_{b\theta_z})$ measured in body-frame (in radians/sec), the flapping angles of rotors, i.e., tip-path-plane orientation angles (in radians) denoted by a_{11} and b_{11} for rotor MR1 and a_{12} and b_{12} for rotor MR2, and the RPM of the two rotors (in revolutions per minute) denoted by RPM_{MR}. Throughout, for brevity, we use the notations $c_x = \cos(\theta_x)$, $s_x = \sin(\theta_x)$, $t_x = \tan(\theta_x)$, etc.

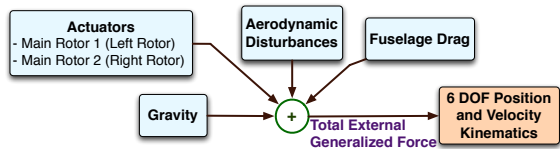Seven control inputs (throttle of both rotors; collective, roll cyclic, and pitch cyclic of each rotor) are

Fig. 4. 6DOF modeling of a twin-rotor aircraft.

Fig. 5. Aerodynamic disturbance model via second-order transfer functions with time-varying coefficients (signal flow for one control input shown).

available: MR1_collective, MR2_collective, MR1_rollcyclic, MR2_rollcyclic, MR1_pitchcyclic, MR2_pitchcyclic, and the throttle. The body-fixed frame is constructed with X axis pointed towards the aircraft nose, Y axis towards the aircraft right, and Z axis downwards. The earth-fixed frame is constructed such that in the nominal aircraft orientation (level flight), the alignment of the earth-fixed frame is such that the X axis is pointed towards the aircraft nose, the Y axis is pointed towards the aircraft left, and the Z axis is pointed upwards. The net force and torque on the aircraft include contributions from gravity, MR1, MR2, fuselage, and wind. The force and torque computations for MR1, MR2, and fuselage are based on the Heffley model and autogyro theory as applied to a twin-rotor aircraft operating in helicopter mode [6,7]. The rotor RPM dynamics are modeled as a first-order lag from the throttle input. The additional dynamics due to the presence of a human pilot has a similar structure as the baseline controller shown in Figure 2 and can be viewed as a parallel interconnection with the flight controller The additive perturbations into the rotorcraft control inputs due to pilot-in-the-loop can be modeled [5] via a third-order transfer function which includes a second-order transfer function for neuromuscular dynamics and a first-order transfer function for the outer-loop pilot command model.

The aerodynamic forces and torques experienced by the rotorcraft in the presence of a ship are modeled in terms of transfer functions (see Figure 5) from a unity covariance white noise to the rotorcraft control inputs that reflect approximately the turbulence effects seen by the rotorcraft. For instance, the MR1_collective input is modeled as perturbed by an additive deflection $\delta_{\text{MR1\_collective}}$ which is modeled as

$$\frac{\delta_{\text{MR1\_collective}}}{w}(s) = \frac{\sum_{i=0}^{1} \eta_{\text{MR1\_collective},i} s^i}{s^2 + \sum_{i=0}^{1} \zeta_{\text{MR1\_collective},i} s^i} \quad (1)$$

where w represents a unity covariance white noise input, and the coefficients in the transfer function on the right hand side of (1) are modeled as functions of the wind speed, ship and rotorcraft geometries, and ship and rotorcraft positions, orientations, and velocities. This model captures the essence of the rotorcraft-ship aerodynamic interactions in a form that is tractable for control design and simulation studies.

While computational fluid dynamics (CFD) models of the ship airwake and deck vortices and their effect on the rotorcraft blade elements would yield more accurate estimates of the aerodynamic disturbance, CFD models are much more complex and are not tractable for use in a control system design setting. Furthermore, CFD characterization of the ship/rotorcraft dynamic interface is still an open and active research problem [1,3,4]. In contrast, the model above is based on a lumped characterization of the aerodynamic effects [2,5] and yields physically realistic estimates of the size and nature of the aerodynamic disturbances, thus providing a viable model for use in control system validation.

III. NONLINEAR ADAPTIVE CONTROLLER

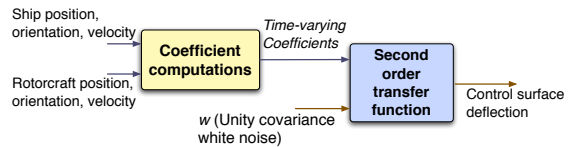The structure of FCS augmentation based on a nonlinear adaptive controller is illustrated in Figure 6. The central

tools used in the design of the augmentation controller are robust adaptive backstepping and ISS concepts [8–11] with the design being based on identifying certain suitable subsystems (of a lower triangular system structure) of the overall aircraft dynamics and exploiting certain ISS properties of the subsystem comprising of the remaining states.

As shown in Figure 6, the FCS augmentation based on the nonlinear adaptive control design technique is comprised of three sub-components: an augmentation for the baseline roll/pitch command generator block, an augmentation for the baseline attitude controller, and an augmentation for the baseline altitude controller. The nonlinear adaptive controller for roll/pitch command generation is designed based on the subsystem with states (x, y, v_{ex}, v_{ey}); the nonlinear adaptive controller for attitude compensation is designed based on the subsystem with states $(\theta_x, \theta_y, \theta_z, v_{b\theta_x}, v_{b\theta_y}, v_{b\theta_z})$; and the nonlinear adaptive controller for the altitude axis is designed based on the subsystem with states (z, v_{ez}) where (v_{ex}, v_{ey}, v_{ez}) is the linear velocity expressed in earth-fixed frame. It can also be shown that the states corresponding to the tip-path-plane orientation and the rotor RPM can be considered as ISS input unmodeled dynamics. From the dynamics of the flapping angles [6,7], it is seen that the dynamics of $[a_{11}, b_{11}]^T$, for instance, can be written as

$$\begin{bmatrix} \dot{a}_{11} \\ \dot{b}_{11} \end{bmatrix} = A_{ab1}(\Omega_{\text{MR}}) \begin{bmatrix} a_{11} \\ b_{11} \end{bmatrix}$$
$$+ B_{ab1}(\Omega_{\text{MR}}) \begin{bmatrix} \text{MR1\_rollcyclic} \\ \text{MR1\_pitchcyclic} \end{bmatrix}$$
$$+ Q_{ab1}(\Omega_{\text{MR}}, v_{bx}, v_{by}, v_{b\theta_x}, v_{b\theta_y}) \quad (2)$$

where Ω_{MR} is the angular velocity of the rotors measured in rad/sec. The dynamics of (a_{12}, b_{12}) can be written similarly featuring matrices A_{ab2}, B_{ab2}, and Q_{ab2}. Based on the physically meaningful range of the coefficients appearing in A_{ab1} and A_{ab2}, it can be shown that A_{ab1} and A_{ab2} are stable matrices; hence, the dynamics of (a_{11}, b_{11}) and (a_{12}, b_{12}) can be considered as stable input unmodeled dynamics for the purposes of control design. Furthermore, it can also be shown that, relative to the "inputs" $(\Omega_{\text{MR}}, v_{bx}, v_{by}, v_{b\theta_x}, v_{b\theta_y})$ which enter into the dynamics of the flapping angles via the matrices $A_{ab1}, B_{ab1}, Q_{ab1}, A_{ab2}, B_{ab2}$, and Q_{ab2}, the dynamics of the subsystem with states $(a_{11}, b_{11}, a_{12}, b_{12})$ are ISS. It can also be shown that the subsystem comprising of the single state, the rotor RPM, can also be viewed as a stable input unmodeled dynamics driven by the throttle input. Thus, the overall 17th order dynamic model of the twin-rotor aircraft can be considered (see Figure 7) as composed of a 12th order core consisting of the rigid-body dynamics and 5th order input unmodeled dynamics. In this context, it is important to note that the intrinsic robustness and adaptation properties of the nonlinear adaptive controller design can accomodate much richer input dynamics without requiring a redesign of the controller.

Nonlinear adaptive attitude controller: The dynamics of the subsystem with state comprising of the angular position $(p_r = [\theta_x, \theta_y, \theta_z]^T)$ and angular velocity $(v_r = [v_{b\theta_x}, v_{b\theta_y}, v_{b\theta_z}])$ can be written as

$$\dot{p}_r = J_r(p_r)v_r \ , \ \dot{v}_r = I_{RB}^{-1}(\tau + \tilde{\tau}) \quad (3)$$
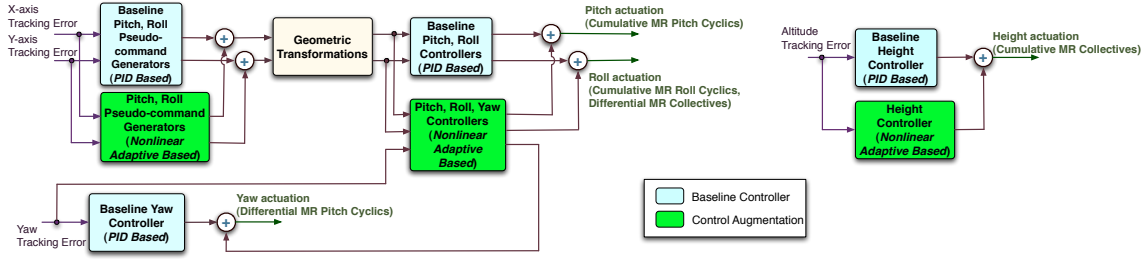
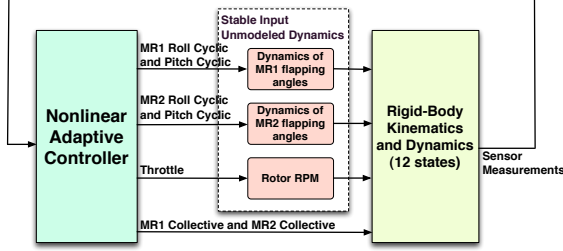Fig. 6.   Structure of nonlinear adaptive controller augmentation.

Fig. 7.   Twin-rotor dynamic model viewed as decomposition into a 12-state rigid body kinematic/dynamic model and stable input unmodeled dynamics.

where $J_r(p_r)$ is the angular velocity Jacobian matrix (dependent on p_r), $\tilde{\tau}$ is a lumped characterization of torques due to various aerodynamic and rigid-body effects, and τ is the (appropriately scaled) torque vector capturing the contributions of the rotors to the roll, pitch, and yaw axes torques. The nonlinear adaptive control design will be presented below with an adaptation for the inertia matrix I_{RB} and with robustness incorporated to handle $\tilde{\tau}$. The attitude controller is designed based on a two-step robust adaptive backstepping procedure. In the first step, the state p_r is addressed and v_r is viewed as a *virtual control input* driving the dynamics of p_r; a *virtual control law* v_r^* for v_r is designed to make p_r track its reference trajectory $p_{r,ref} = [\theta_{x,ref}, \theta_{y,ref}, \theta_{z,ref}]^T$. In the second step, the error between v_r and v_r^* is considered and the control law for the input τ is designed to make the error $(v_r - v_r^*)$ small. Finally, a commutation procedure is used to translate the control law for τ into control laws in terms of the rotor pitch, roll, and collective inputs.

Step 1: In the first step of backstepping, the Lyapunov function $V_1 = \tilde{p}_r^T Q_{pr} \tilde{p}_r$ is used where $\tilde{p}_r = p_r - p_{r,ref}$ and Q_{pr} is a 3×3 positive-definite matrix which can be used to tune the controller performance. Defining $\tilde{v}_r = v_r - v_r^*$ where $v_r^* = J_r^{-1}(\dot{p}_{r,ref} - K_{pr}\tilde{p}_r)$ with K_{pr} being a 3×3 gain matrix which must be picked such that $Q_{pr}K_{pr} + K_{pr}^T Q_{pr} \geq \nu_1 I_{3\times3}$ where $I_{3\times3}$ denotes the 3×3 identity matrix and ν_1 is any positive constant, we obtain the Lyapunov inequality $\dot{V}_1 \leq -\nu_1||\tilde{p}_r||^2 + 2\tilde{p}_r^T Q_{pr} J_r \tilde{v}_r$. Since Q_{pr} is a positive-definite matrix, it is evident that a matrix K_{pr} can be picked to satisfy the prescribed condition.

Step 2: A new Lyapunov function is defined as $V_2 = V_1 + \tilde{v}_r^T I_{RB} \tilde{v}_r$ differentiating which

$$\dot{V}_2 \leq -\nu_1||\tilde{p}_r||^2 + 2\tilde{p}_r^T Q_{pr} J_r \tilde{v}_r + 2\tilde{v}_r^T(\tau + \tilde{\tau})$$
$$+2\tilde{v}_r^T I_{RB}\left[- \overbrace{J_r^{-1}}(\dot{p}_{r,ref} - K_{pr}\tilde{p}_r) \right.$$
$$\left. -(J_r^{-1})[\ddot{p}_{r,ref} - K_{pr}(J_r v_r - \dot{p}_{r,ref})] \right]. \quad (4)$$

Define
$$\zeta_r = -\overbrace{J_r^{-1}}(\dot{p}_{r,ref} - K_{pr}\tilde{p}_r) - (J_r^{-1})[\ddot{p}_{r,ref} - K_{pr}(J_r v_r - \dot{p}_{r,ref})].$$
Then, the terms in the second line of (4) reduce to simply $2\tilde{v}_r^T I_{RB} \zeta_r$. Using the Kronecker algebra property that with

any three matrices $A \in \mathcal{R}^{n\times m}$, $X \in \mathcal{R}^{m\times p}$, and $B \in \mathcal{R}^{p\times q}$, the property $\text{vec}(AXB) = (B^T \otimes A)\text{vec}(X)$ holds, we obtain $2\tilde{v}_r^T I_{RB} \zeta_r = 2(\zeta_r^T \otimes \tilde{v}_r^T)\text{vec}(I_{RB})$ where $\otimes$ denotes the Kronecker product and vec denotes the vector operator which is defined as the vector formed by stacking the columns of its matrix argument. Design $\tau = \tau^*$ with

$$\tau^* = -K_{dr}\tilde{v}_r + \text{mat}_3(\hat{\xi}_r)\Big[\overbrace{J_r^{-1}}(\dot{p}_{r,ref} - K_{pr}\tilde{p}_r)$$
$$+ (J_r^{-1})[\ddot{p}_{r,ref} - K_{pr}(J_r v_r - \dot{p}_{r,ref})] \Big] - J_r^T Q_{pr}^T \tilde{p}_r \quad (5)$$

where K_{dr} is a 3×3 positive-definite controller gain matrix (K_{dr} could be picked as a function of all measured states), $\hat{\xi}_r$ is an adaptation vector of dimension 9×1, and mat_3 denotes the matrix reshaping operator defined for a vector $\omega = [\omega_1, \omega_2, \ldots, \omega_9] \in \mathcal{R}^9$ as the matrix with $(i,j)^{th}$ element $\omega_{i+3*(j-1)}$. The dynamics of $\hat{\xi}_r$ are designed as
$$\dot{\hat{\xi}}_r = \Gamma_{\xi_r}^{-1}[\zeta_r^T \otimes \tilde{v}_r^T]^T \quad (6)$$
where Γ_{ξ_r} is a 9×9 gain matrix which should be picked as a positive-definite matrix. Defining the Lyapunov function $V = V_2 + \tilde{\xi}_r^T \Gamma_{\xi_r} \tilde{\xi}_r$ where $\tilde{\xi}_r = \hat{\xi}_r - \text{vec}(I_{RB})$, it is seen from the definition of τ^* in (5), the adaptation dynamics in (6), and the fact that $2\tilde{v}_r^T \tilde{\tau} \leq \tilde{v}_r^T K_{dr} \tilde{v}_r + \tilde{\tau}^T K_{dr}^{-1}\tilde{\tau}$, that
$$\dot{V} \leq -\nu_1||\tilde{p}_r||^2 - \tilde{v}_r^T K_{dr}\tilde{v}_r + \tilde{\tau}^T K_{dr}^{-1}\tilde{\tau}. \quad (7)$$

From (7), noting that $\tilde{\tau}$ can be captured within some (possibly state-dependent) bound over the range of operating conditions, it follows by standard Lyapunov auguments that $||\tilde{p}_r||$ and $||\tilde{v}_r||$ can be regulated to a small neighborhood of the origin if K_{pr} and K_{dr} are picked sufficiently large. In general, K_{dr} could be picked to depend on any measured state variable for simple gain-scheduling; the utility of such gain-scheduling has been noted in simulations to be primarily relative to p_r wherein K_{dr} is picked to be dependent on p_r with a larger value of p_r resulting in a smaller value of K_{dr}.

Remark 1: In implementation, a σ-modification is utilized to guard against adaptation parameter drift instability, i.e., the dynamics (6) are replaced by $\dot{\hat{\xi}}_r = -\sigma_{\xi_r}\hat{\xi}_r + \Gamma_{\xi_r}^{-1}[\zeta_r^T \otimes \tilde{v}_r^T]^T$ with σ_{ξ_r} being a 9×9 matrix chosen such that $\Gamma_{\xi_r}\sigma_{\xi_r} + \sigma_{\xi_r}^T \Gamma_{\xi_r} \geq \nu_{\xi_r} I_{9\times9}$ where ν_{ξ_r} is a positive constant. Since Γ_{ξ_r} is a positive-definite matrix, such a choice of σ_{ξ_r} is always possible. The additional term $-\sigma_{\xi_r}\hat{\xi}_r$ introduced provides a stabilizing effect in the adaptation dynamics.

Remark 2: While the Lyapunov analysis above addressed uncertainty in the inertia matrix, it can be shown that the adaptation in the designed controller actually addresses a lumped characterization of system uncertainty including unmodeled nonlinearities and changing environmental conditions. It is also worthwhile to note that while $\hat{\xi}_r$ is of dimension 9×1 in the design presented above, its elements which contribute most to controller performance are entries corresponding to diagonal elements of $\text{mat}_3(\hat{\xi}_r)$, i.e., the first, fifth, and ninth elements of $\hat{\xi}_r$. Hence, the controller dynamic order can be reduced by incorporating dynamic adaptations

only for these elements. In this case, the adaptation vector $\hat{\xi}_r$ is of dimension 3×1 and τ^* is designed as

$$\tau^* = -K_{dr}\tilde{v}_r + \text{diag}(\hat{\xi}_r)\left[\overbrace{J_r^{-1}}(\dot{p}_{r,ref} - K_{pr}\tilde{p}_r)\right.$$
$$\left. +(J_r^{-1})[\ddot{p}_{r,ref} - K_{pr}(J_r v_r - \dot{p}_{r,ref})]\right] - J_r^T Q_{pr}^T \tilde{p}_r \quad (8)$$

where $\text{diag}(\hat{\xi}_r)$ denotes the 3×3 matrix with its diagonal elements being the entries of $\hat{\xi}_r$ and with zeros elsewhere. The dynamics of $\hat{\xi}_r$ are designed as

$$\dot{\hat{\xi}}_r = -\sigma_{\xi_r}\hat{\xi}_r + \Gamma_{\xi_r}^{-1}[\zeta_{r,1}\tilde{v}_{r,1}, \zeta_{r,2}\tilde{v}_{r,2}, \zeta_{r,3}\tilde{v}_{r,3}]^T \quad (9)$$

where $\zeta_{r,i}, i = 1, 2, 3$ are the elements of ζ_r, $\tilde{v}_{r,i}, i = 1, 2, 3$ are the elements of $\tilde{v}_r$, Γ_{ξ_r} is a 3×3 positive-definite gain matrix and σ_{ξ_r} is a 3×3 matrix which should be chosen such that $\Gamma_{\xi_r}\sigma_{\xi_r} + \sigma_{\xi_r}^T\Gamma_{\xi_r} \geq \nu_{\xi_r}I_{3\times 3}$ with ν_{ξ_r} being a positive constant. In (9), the σ-modification described in Remark 1 has also been incorporated.

Nonlinear adaptive roll/pitch command generator: The objective of the roll/pitch command generator design is to construct roll and pitch reference signals to make (x, y) track given reference signals (x_{ref}, y_{ref}). The backstepping based design is carried out in two steps. In the first step, the states (x, y) are considered and the states (v_{ex}, v_{ey}) are considered as virtual control inputs. In the second step, roll and pitch signals are considered as the control inputs and are designed to regulate the signals (v_{ex}, v_{ey}) to the values of their designed virtual control laws. Carrying out the design along analogous lines to the design of the attitude controller presented earlier, the roll/pitch command reference signals (θ_x^*, θ_y^*) are designed via the following equations

$$p_p = [x, y]^T, \; \tilde{p}_p = p_p - p_{p,ref}, \; p_{p,ref} = [x_{ref}, y_{ref}]^T$$
$$v_{ep} = [v_{ex}, v_{ey}]^T, \; v_{ep}^* = -K_{pp}\tilde{p}_p + \dot{p}_{p,ref}, \; \tilde{v}_{ep} = v_{ep} - v_{ep}^*$$
$$\bar{\theta}_p = -K_{dp}\tilde{v}_{ep} - \tilde{K}_{pp}\tilde{p}_p - \hat{\xi}_p[K_{pp}(v_{ep} - \dot{p}_{p,ref}) - \ddot{p}_{p,ref}]$$
$$\dot{\hat{\xi}}_p = -\sigma_{\xi_p}\hat{\xi}_p + \Gamma_{\xi_p}\tilde{v}_{ep}[K_{pp}(v_{ep} - \dot{p}_{p,ref}) - \ddot{p}_{p,ref}]$$
$$\begin{bmatrix} \theta_x^* \\ \theta_y^* \end{bmatrix} = \begin{bmatrix} 0 & -1 \\ 1 & 0 \end{bmatrix}(R_e^b)^T\bar{\theta}_p \quad (10)$$

where R_e^b is the rotation matrix relating the earth frame to the body frame, K_{pp}, $\tilde{K}_{pp}$, K_{dp}, σ_{ξ_p}, and Γ_{ξ_p} are controller gains which should be picked to be positive numbers, and $\hat{\xi}_p$ is a 2×1 adaptation vector which addresses a lumped characterization of overall system uncertainty in roll/pitch contribution to the dynamics of (x, y) degrees of freedom.

Nonlinear adaptive altitude controller: The altitude controller is designed using the subsystem comprising of the states (z, v_{ez}) with the objective being to track a given altitude reference signal z_{ref}. Carrying out the backstepping based design along analogous lines to the design of the attitude controller presented earlier, the altitude control law is designed in terms of d_z^* as

$$\tilde{z} = z - z_{ref}, \; v_{ez}^* = -K_{pz}\tilde{z} + \dot{z}_{ref}, \; \tilde{v}_{ez} = v_{ez} - v_{ez}^*$$
$$d_z^* = K_{dz}\tilde{v}_{ez} + \tilde{K}_{pz}\tilde{z} + \hat{\xi}_z[K_{pz}(v_{ez} - \dot{z}_{ref}) - \ddot{z}_{ref}]$$
$$\dot{\hat{\xi}}_z = -\sigma_{\xi_z}\hat{\xi}_z + \Gamma_{\xi_z}\tilde{v}_{ez}[K_{pz}(v_{ez} - \dot{z}_{ref}) - \ddot{z}_{ref}] \quad (11)$$

where K_{pz}, $\tilde{K}_{pz}$, K_{dz}, σ_{ξ_z}, and Γ_{ξ_z} are controller gains which should be picked to be positive numbers and $\hat{\xi}_z$ is a scalar adaptation signal.

Commutation: MR1_collective, MR2_collective, MR1_rollcyclic, MR2_rollcyclic, MR1_pitchcyclic, and

MR2_pitchcyclic are computed based on d_z^* and τ as:

$$\text{MR1\_collective} = \frac{d_z^* - \tau_{\text{roll}}}{2} + \text{TMR1\_collective}$$

$$\text{MR2\_collective} = \frac{d_z^* + \tau_{\text{roll}}}{2} + \text{TMR2\_collective}$$

$$\text{MR1\_rollcyclic} = \tau_{\text{roll}} + \text{TMR1\_rollcyclic}$$

$$\text{MR2\_rollcyclic} = \tau_{\text{roll}} + \text{TMR2\_rollcyclic}$$

$$\text{MR1\_pitchcyclic} = \frac{\tau_{\text{pitch}} + \tau_{\text{yaw}}}{2} + \text{TMR1\_pitchcyclic}$$

$$\text{MR2\_pitchcyclic} = \frac{\tau_{\text{pitch}} - \tau_{\text{yaw}}}{2} + \text{TMR2\_pitchcyclic}$$

where TMR1_collective, etc., are the trim values for the aircraft. The commutation described above prescribes a control allocation mapping the four control signals $(\tau_{\text{roll}}, \tau_{\text{pitch}}, \tau_{\text{yaw}}, d_z^*)$ to the six control surface signals (MR1_collective, MR2_collective, MR1_rollcyclic, MR2_rollcyclic, MR1_pitchcyclic, MR2_pitchcyclic). For better performance and to avoid one degree of freedom from dominating over another in the computation of a control input that they share, saturations with appropriate saturation levels can be incorporated into the terms of the commutation laws. Also, the control inputs are saturated to appropriate levels before feeding into the servos.

IV. θ-D BASED CONTROLLER

In this section, an augmentation scheme which utilizes a θ-D based controller [12–15] is described. The structure of the FCS augmentation with the θ-D based controller is shown in Figure 8. The θ-D approach is based on casting a nonlinear system as a *pseudo-linear* system with state-dependent system matrices and then using an SDRE to design the control law. In contrast, however, with solving the SDRE at every sampling instant which would be computationally very burdensome, the θ-D approach relies on an iterative approximate solution of the SDRE using a reformulation of the pseudo-linear system as the combination of a nominal part and a perturbation part. This procedure essentially replaces the Riccati equation with a Lyapunov equation. Since a Lyapunov equation is computationally much simpler to solve than a Riccati equation, the θ-D approach yields a controller with very low computational requirements relative to the original SDRE based controller.

For brevity, as shown in Figure 8, we focus here on the θ-D augmentation for the inner-loop controllers since these are the most critical in shipboard operation. Since the altitude degree of freedom can be handled easily in conjunction with the roll, pitch, and yaw axes in a unified manner, the θ-D augmentation presented here addresses the four degrees of freedom of roll, pitch, yaw, and altitude. Similar θ-D based augmentation controllers could be designed for the roll and pitch command generators if required under the operating conditions. Considering the roll, pitch, yaw, and altitude degrees of freedom, the state vector for control design purposes is given by $x_{IL} = [v_{b\theta_x}, v_{b\theta_y}, v_{b\theta_z}, \theta_x, \theta_y, \theta_z, v_{ez}, z]^T$. The input vector is formulated as $u_{IL} = [\delta_c, \delta_p, \delta_q, \delta_r]^T$ where (see Figure 8) δ_c, δ_p, δ_q, and δ_r are the contributions of the θ-D controller to the altitude, roll, pitch, and yaw axis actuations, respectively. To formulate the SDRE, the system with state x_{IL} is first written in the form

$$\dot{x}_{IL} = A_{IL}(x_{IL})x_{IL} + B_{IL}(x_{IL})u_{IL} + \tilde{F}_{IL} \quad (12)$$

where A_{IL} and B_{IL} are state-dependent matrices of dimensions 8×8 and 8×4, respectively, and $\tilde{F}_{IL}$ is an 8×1 vector which denotes a lumped characterization of various aerodynamic and rigid-body effects. Considering a
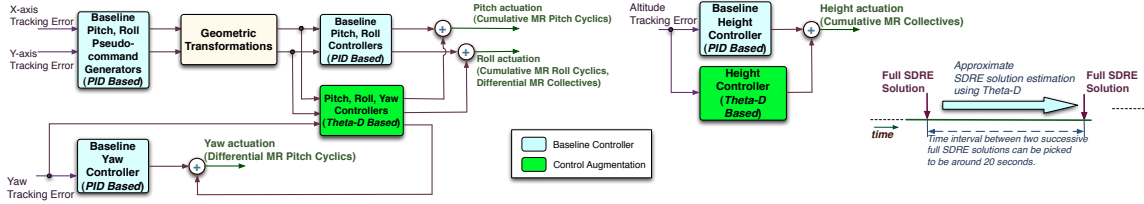
Fig. 8.   Structure of θ-D controller augmentation.

decomposition of the state vector x_{IL} into its constituent attitude and altitude components as $x_{IL} = [v_{b\theta}^T, \theta^T, v_{ez}, z]^T$ where $v_b = [v_{b\theta_x}, v_{b\theta_y}, v_{b\theta_z}]^T$ and $\theta = [\theta_x, \theta_y, \theta_z]^T$, using the dynamic model described in Section II, relegating various aerodynamic and rigid-body terms to $\tilde{F}_{IL}$ to be handled through the robustness margin of the θ-D controller, and examining the axes through which the control inputs enter into the system, it can be shown that

$$A_{IL} = \begin{bmatrix} I_{RB}^{-1} S(I_{RB} v_{b\theta}) & 0_{3\times3} & 0_{3\times1} & 0_{3\times1} \\ J_r & 0_{3\times3} & 0_{3\times1} & 0_{3\times1} \\ 0_{1\times3} & 0_{1\times3} & 0 & 0 \\ 0_{1\times3} & 0_{1\times3} & 1 & 0 \end{bmatrix}$$

$$B_{IL} = \begin{bmatrix} B_{v_{b\theta}, IL} \\ 0_{3\times4} \\ [1,0,0,0] \\ 0_{1\times4} \end{bmatrix} ; \quad B_{v_{b\theta}, IL} = \begin{bmatrix} 0 & 1 & 0 & 0 \\ 0 & 0 & -1 & 0 \\ 0 & 0 & 0 & -1 \end{bmatrix} \quad (13)$$

where J_r is the angular velocity Jacobian, I_{RB} is the 3×3 inertia matrix, and $S(\omega)$ with $\omega = [\omega_x, \omega_y, \omega_z]^T$ denotes the skew-symmetric matrix of ω.

Given a pseudo-linear system description $\dot{x} = A(x)x + B(x)u$, the stabilizing controller that minimizes the quadratic cost $J = \frac{1}{2} \int_0^\infty (x^T Q x + u^T R u) dt$ with Q being a positive semi-definite matrix of dimension $n \times n$ and R being a positive definite matrix of dimension $m \times m$, is given by $u = -R^{-1} B^T(x) P(x) x$ where $P(x)$ is a symmetric $n \times n$ matrix computed as the solution to the SDRE $P(x)A(x) + A^T(x)P(x) - P(x)B(x)R^{-1}B^T(x)P(x) + Q = 0$. The controller based on solving the SDRE at every controller sampling instant is computationally very expensive. The θ-D technique addresses this computational intractability of the SDRE approach by replacing on-line calculation of the SDRE with an approximate closed-form solution based on a power series representation of the form $P(x) \approx \sum_{i=0}^{n_{\theta D}} T_i \theta^i$ where $T_0, \ldots, T_n$ are $n \times n$ symmetric matrices, θ is any positive constant, and $n_{\theta D}$ is a positive integer indicating the number of terms in the power series expansion. The matrices $T_0, \ldots, T_n$ are computed based on a perturbation of the cost function of the form $J = \frac{1}{2} \int_0^\infty (x^T [Q + \sum_{i=1}^{n_{\theta D}} D_i \theta^i] x + u^T R u) dt$ using the method described in [12–15].

V. SIMULATION STUDIES

A simulation package has been developed for the overall dynamic system formed by a twin-rotor aircraft operating in a shipboard environment (including the ship/rotorcraft dynamic interface and the human pilot in the loop) based on the dynamic model illustrated in Figure 3. In developing the simulation platform, IntelliTech's high-fidelity 6DOF ship dynamic simulator [16] was leveraged and a 6DOF dynamic model of the rotorcraft was implemented along the lines described in Section II. The dynamics of the twin-rotor aircraft and the ship were implemented in C++ while the remaining components of the overall dynamic simulator and the controllers were implemented in Matlab. The overall system was hooked together in Simulink using the S-function interface for the C++ implementations of the dynamics of the rotorcraft and the ship. A 3D visualization environment was also implemented using OpenGL (see screenshots in

Figure 9). The visualization environment shows the positions and orientations of both the ship and the twin-rotor aircraft and provides full pan, tilt, and zoom capabilities.
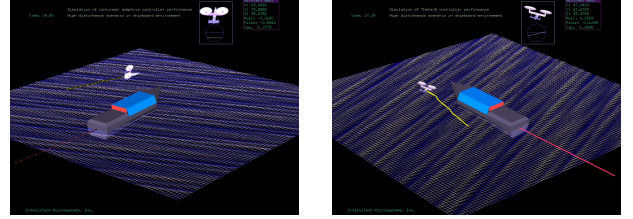

Fig. 9.   Screenshots of the 3D visualization environment for twin-rotor aircraft operation in shipboard environment.

A. Simulation studies with the nonlinear adaptive controller

The performance of the nonlinear adaptive controller is evaluated in this section using a test case wherein the twin-rotor aircraft is commanded to track the position and yaw reference trajectories described by the equations (where positions are in feet and angle is in radians) $x_{ref}(t) = 100 + 50 \sin(0.01t)$, $y_{ref}(t) = 50 + 50 \sin(0.06t)$, $z_{ref}(t) = 20 + 3 \sin(0.04t)$, and $\theta_{z,ref}(t) = 0.1 \sin(0.03t)$. A ship is introduced into the environment with its trajectory being such that it would pass directly under the aircraft around time 156 seconds. Based on the disturbance modeling outlined in Section II, this results in the injection of disturbance forces of magnitude around 14000 lb-force and disturbance torques of magnitude around 1200 ft lb-force. It is seen from Figure 10 that the aircraft would lose stability at around 160 seconds if the baseline controller is used without a controller augmentation (this level of disturbance which reflects an environment at the high end of sea state 3 exceeds the maximum level of disturbance that the baseline controller can handle alone by around 40%). With the nonlinear adaptive controller added in as an augmentation controller, it is seen from Figure 11 that the aircraft stability is preserved even in the face of severe aerodynamic disturbances.
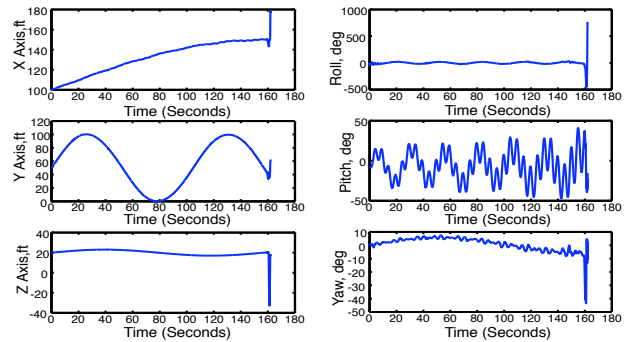

Fig. 10.   Instability seen with baseline controller.

B. Simulation studies with the θ-D based controller

While the static fixed-gain PID controller is not able to retain stability when large roll and pitch motions are
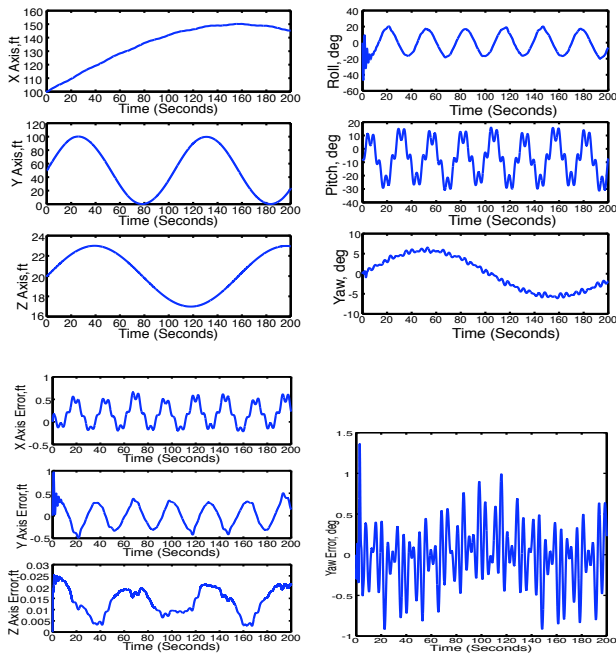
Fig. 11. FCS performance with nonlinear adaptive controller augmentation.

caused due to high disturbance conditions in the test case presented in Section V-A, the θ-D based controller is able to adjust gains in real-time to retain stability. While the point-wise eigenvalues of a time-varying nonlinear system do not necessarily relate directly to system stability, it is nevertheless interesting to observe the variation of closed-loop eigenvalues as illustrated in Figure 12; note that the θ-D controller is able to maintain the eigenvalues in the left half plane through approximate solution of the SDRE. In the absence of θ-D augmentation, the eigenvalues would be shifted to the right half plane.
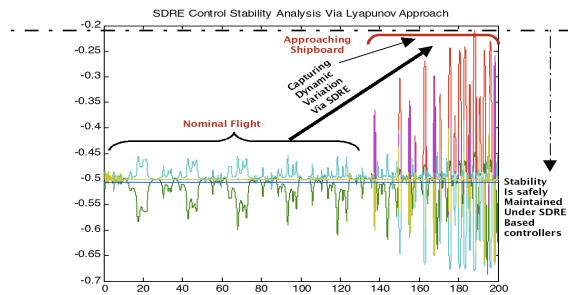

Fig. 12. Dynamic poles shifting under high disturbance.

The closed-loop behavior of the twin-rotor aircraft with controller augmentation is illustrated in Figure 13 for two cases. In the first case, the augmentation controller is a direct Linear Quadratic Regulator (LQR), i.e., on-line solution of the SDRE at every sampling instant, and in the second case, the proposed θ-D controller is used as the augmentation controller. It is seen that the θ-D controller actually provides a smoother response than the straightforward LQR solver due to the smoothing nature of the power series representation used in the θ-D controller which tends to not excite higher frequency modes in the dynamics. Furthermore, the computational burden of the θ-D controller is very small relative to the full SDRE solution, typically requiring less than 3% computational time per controller sample. The computational burden of the nonlinear adaptive controller is even lower (less than 2% computational time per controller sample as
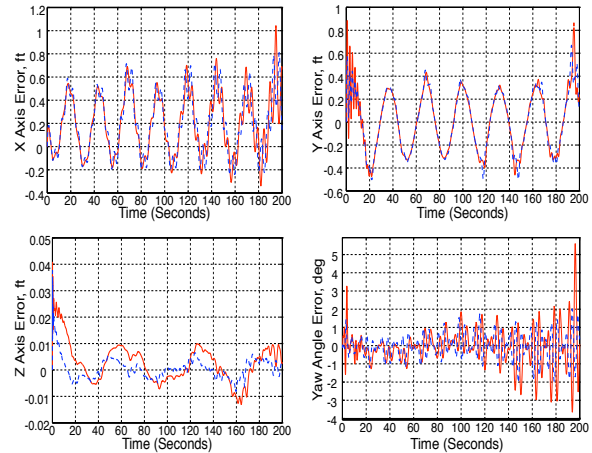
compared to the full SDRE solver).

Fig. 13. FCS performance with augmentation using full SDRE based controller (red solid line) and using θ-D controller (blue dashed line).

VI. CONCLUSION

Two techniques for FCS augmentation for robustness and stability enhancement of the twin-rotor aircraft have been developed and demonstrated through simulation studies. The proposed FCS augmentation design techniques promise significant improvements in performance, robustness, and stability of the aircraft flight under severe aerodynamic disturbances, and also enhance the operational envelope of shipboard operations to a wider range of sea conditions and ship and rotorcraft motions.

REFERENCES

[1] D. Carico, "Rotorcraft shipboard flight test analytic options," in *Proc. IEEE Aerospace Conf.*, Mar. 2004.
[2] J. A. Lusardi, *Control equivalent turbulence inputs model for the UH-60*. Univ. of California, Davis, CA: Ph.D. Dissertation, 2004.
[3] D. Lee, *Simulation and control of a helicopter operating in a ship airwake*. Penn State University: Ph.D. Dissertation, 2005.
[4] S. Polsky, "Progress towards modeling ship/aircraft dynamic interface," in *Proc. HPCMP Users Group Conf.*, 2006.
[5] R. A. Hess, "Simplified technique for modeling piloted rotorcraft operations near ships," *Journal of Guidance, Control, and Dynamics*, vol. 29, Nov.-Dec. 2006.
[6] R. Heffley and M. Mnich, "Minimum complexity helicopter simulation math model," NASA, Tech. Rep. 177476, April 1988.
[7] T. L. Ng, P. Krishnamurthy, F. Khorrami, and S. Fujikawa, "Autonomous flight control and hardware-in-the-loop simulator for a small helicopter," in *Proc. IFAC WC*, Prague, Czech Republic, July 2005.
[8] M. Krstić, I. Kanellakopoulos, and P. V. Kokotović, *Nonlinear and Adaptive Control Design*. New York: Wiley, 1995.
[9] E. Sontag, "The ISS philosophy as a unifying framework for stability-like behavior," in *Nonlinear control in the Year 2000*, ser. Lecture Notes in Control and Information Sciences. Berlin: Springer Verlag, 2000, vol. 2, pp. 443–468.
[10] F. Khorrami, P. Krishnamurthy, and H. Melkote, *Modeling and Adaptive Nonlinear Control of Electric Motors*. New York: Springer Verlag, 2003.
[11] P. Krishnamurthy and F. Khorrami, "Dynamic high-gain scaling: state and output feedback with application to systems with ISS appended dynamics driven by all states," *IEEE Trans. on Automatic Control*, vol. 49, pp. 2219–2239, Dec. 2004.
[12] M. Xin, S. N. Balakrishnan, D. T. Stansbery, and E. J. Ohlmeyer, "Nonlinear missile autopilot design with theta-D technique," *Journal of Guidance, Control, and Dynamics*, vol. 27, 2004.
[13] D. Drake, M. Xin, and S. N. Balakrishnan, "New nonlinear control technique for ascent phase of reusable launch vehicles," *Journal of Guidance, Control, and Dynamics*, vol. 27, 2004.
[14] M. Xin and S. N. Balakrishnan, "A new method for suboptimal control of a class of nonlinear systems," *Optimal Control Applications and Methods*, vol. 26, pp. 55–83, 2005.
[15] Q. Lam, D. Drake, and B. Ridgely, "Input saturation treatments: a performance comparison of direct adaptive control and $\theta - D$ control methodologies," in *Proc. IEEE Aero. Conf.*, Big Sky, MO, Mar. 2007.
[16] P. Krishnamurthy, F. Khorrami, and T. L. Ng, "Control design for unmanned sea surface vehicles: Hardware-in-the-loop simulator and experimental results," in *Proc. 2007 International Conf. on Intelligent Robots and Systems*, San Diego, CA, Oct. 2007.